Inorganic Chemistry

pubs.acs.org/IC Article

Coordination of Ru(II)-Arene Fragments to Dipyridophenazine Ligands Leads to the Modulation of Their In Vitro and In Vivo Anticancer Activity

Stefan Nikolić, Jemma Arakelyan, Vladimir Kushnarev, Samah Mutasim Alfadul, Dalibor Stanković, Yaroslav I. Kraynik, Sanja Grgurić-Šipka,* and Maria V. Babak*

Cite This: *Inorg. Chem.* 2023, 62, 8188–8199 Read Online

ACCESS | Metrics & More | Article Recommendations | Supporting Information

ABSTRACT: Despite extensive research on the anticancer properties of Ru complexes with dipyrido[3,2-*a*:2′,3′-*c*]phenazine (dppz) ligands, their in vivo efficacy is rarely investigated. Aiming to understand whether the coordination of certain half-sandwich Ru(II)-arene fragments might improve the therapeutic potential of dppz ligands, we prepared a series of Ru(II)-arene complexes with the general formula $[(\eta^6\text{-arene})Ru(dppz\text{-}R)Cl]PF_6$, where the arene fragment was benzene, toluene, or *p*-cymene and R was $-NO_2$, -Me, or -COOMe. All compounds were fully characterized by ^1H and ^{13}C NMR spectroscopy and high-resolution ESI mass-spectrometry, and their purity was verified by elemental analysis. The electrochemical activity was investigated using cyclic voltammetry. The anticancer activity of dppz ligands and their respective Ru complexes was assessed against several cancer cell lines, and their selectivity toward cancer cells was assessed using healthy MRC5 lung fibroblasts. The substitution of benzene with a *p*-cymene fragment resulted in a more than 17-fold increase of anticancer activity and selectivity of Ru complexes and significantly enhanced DNA degradation in HCT116 cells. All Ru complexes were electrochemically active in the biologically accessible redox window and were shown to markedly induce the production of ROS in mitochondria. The lead Ru-dppz complex significantly reduced tumor burden in mice with colorectal cancers without inducing liver and kidney toxicity.

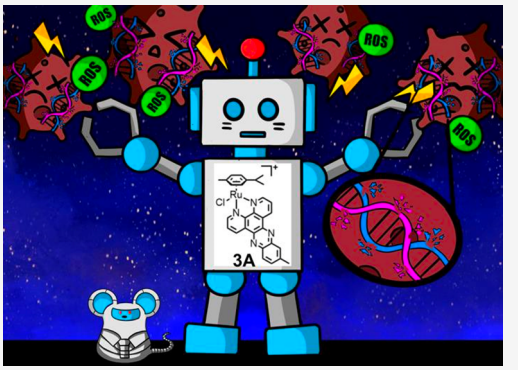

INTRODUCTION

Anticancer Ru complexes gained significant interest after two iconic Ru(III) complexes—NAMI-A ((ImH)[*trans*-$RuCl_4$(dmso-S)(Im)], Im = imidazole) and KP1339 (later renamed as IT-139 and BOLD-100, Na[*trans*-$RuCl_4(Ind)_2$], Ind = indazole)—entered their first human clinical trials at the beginning of the 21st century.[1] Half-sandwich Ru complexes were suggested as alternatives to Ru(III) complexes since their structures could be easily modified according to the required design.[2] Despite the excellent potential of (arene)Ru complexes as anticancer agents, none of them has entered clinical trials so far, probably due to their uncertain mechanism of action.[3] Interestingly, some half-sandwich Ru complexes were shown to exhibit anticancer properties due to their catalytic transfer hydrogenation activity in the reduction of NAD^+ to NADH.[4−6] Other half-sandwich Ru complexes could bypass multidrug resistance and conventional programmed cell death pathways induced by commonly used chemotherapeutic agents.[7,8] Therefore, this class of compounds still remains worthy of investigation.

In the past decades, Ru complexes with dppz ligands have been extensively investigated as molecular imaging probes and phototherapeutic agents due to their unique photophysical properties and excellent DNA binding affinity.[9,10] Interest to the class of Ru(II) complexes with a dppz ligand was motivated by the work of Barton et al., who demonstrated that the $[Ru(bipy)_2(dppz)]^{2+}$ complex could enhance its photoluminescence by several orders of magnitude upon interactions with DNA.[11] Subsequent studies revealed that the structure of the octahedral heteroleptic Ru-dppz complexes could be easily fine-tuned depending on their potential applications. For example, the increase of the size of Ru complexes due to the extension of the aromatic system in the dppz ligand[12] or introduction of several dppz ligands[13] resulted in the significant enhancement of their cytotoxicity. Moreover, slight variations in the structure of the complexes led to the modulation of their intracellular accumulation and respective anticancer mechanism of action. It is believed that the

Received: February 20, 2023
Published: May 18, 2023

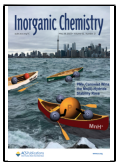

https://doi.org/10.1021/acs.inorgchem.3c00570
Inorg. Chem. 2023, 62, 8188−8199

anticancer activity of (polypyridyl)Ru-dppz complexes originates from their ability to intercalate into duplex DNA;[14−16] however, it was also shown that some of these complexes could readily intercalate into DNA G-quadruplex[17] and RNA triplex[18] or accumulate in mitochondria, thereby initiating mitochondria-mediated apoptosis.[13,19]

In general, the coordination of dppz-derived ligands to the Ru(polypyridyl) backbone yields highly stable Ru complexes that are inert under physiological conditions.[16,20] On the other hand, the use of organometallic fragments typically leads to the formation of half-sandwich metal-dppz complexes with labile chlorido ligands.[21,22] It is believed that the hydrolysis of the labile ligands results in the formation of highly reactive solvato complexes that readily bind to the DNA,[21] leading to DNA degradation. Therefore, various half-sandwich Ru complexes with dppz ligands and its analogues demonstrated promising anticancer activity, which was dependent on their reactivity and interactions with biomolecules. For example, Ru(II)-arene complexes with diimine ligands, where diimine was 1,10-phenanthroline, 5,6-dimethyl-1,10-phenanthroline, dppz, or 11,12-dimethyl-dppz induced oxidative cleavage of the supercoiled DNA plasmid.[23] The most pronounced effects were recorded for complexes with dppz-based ligands and the observed DNA effects were in correlation with the cytotoxicity of the complexes. Interestingly, the DNA-binding efficiency of Ru(II)-arene complexes was not only defined by the chelating ligand but also by the steric bulk of other participating co-ligands.[24] It was shown that Ru(II)-dppz complexes with S-coordinated L-methionine or L-cysteine and bulky η^6-hexamethylbenzene were characterized by the higher K_b values than their η^6-benzene analogues, suggesting stronger duplex stabilization.[24] Previously, some of us reported the synthesis, characterization, and preliminary biological assessment of (arene)Ru complexes with dppz-derived ligands.[25,26] Several complexes demonstrated enhanced cytotoxicity and selectivity in comparison with the clinically used drug cisplatin. In contrast, structurally similar half-sandwich Ru(II) complexes with bipyrimidine, tryptanthrin-6-oxime, or 11*H*-indeno[1,2-*b*]quinoxalin-11-one derivatives were devoid of cytotoxicity[27] or only moderately cytotoxic,[28] indicating the importance of dppz-derived ligands in the biological activity of resulting complexes.

Surprisingly, despite continuous interest in the therapeutic potential of Ru-dppz complexes, the majority of the studies for both heteroleptic and half-sandwich Ru-dppz and structurally similar complexes were mostly limited to in vitro experiments. There are only few examples of in vivo studies with Ru-dppz complexes or uncoordinated dppz-derived ligands. For example, heteroleptic Ru(bipyridine)(dppz) complexes showed high antiproliferative, antimetastatic, and antiangiogenic activity in the MDA-MB-231 zebrafish xenograft model.[29] Another heteroleptic Ru(tetra-imidazole)(dppz) complex significantly inhibited tumor growth in mice xenografted with A549 lung cancer.[19]

In this project, we prepared a series of dppz-derived ligands and respective piano-stool Ru-arene complexes with the general formula $[(\eta^6\text{-arene})Ru(dppz\text{-}R)Cl]PF_6$. We discussed the effects of the arene fragment and substituents in the dppz ligand on the electrochemical and anticancer properties of resulting complexes. We investigated the mechanism of action of the lead drug candidates, including DNA degradation and ROS induction, and linked the electrochemical activity of these complexes with their ability to induce the production of deadly ROS in the mitochondria of cancer cells. Importantly, this work extended the limited in vivo data about the toxicity and antitumor efficacy of Ru-dppz complexes and respective dppz ligands.

EXPERIMENTAL SECTION

Materials and Methods. *Chemicals and Materials.* All chemicals were of reagent-grade quality or higher, obtained from commercial suppliers, and used without further purification. Solvents were used as received. $RuCl_3{\cdot}3H_2O$ was purchased from Johnson Matthey (London, United Kingdom). $[(\eta^6\text{-}p\text{-Cymene})RuCl_2]_2$, $[(\eta^6\text{-toluene})RuCl_2]_2$, and $[(\eta^6\text{-benzene})RuCl_2]_2$ were prepared according to a published procedure.[30] Thiazolyl blue tetrazolium bromide (MTT) was purchased from Alfa Aesar; Roswell Park Memorial Institute (RPMI 1640) medium, Dulbecco's modified Eagle's medium (DMEM) medium, fetal bovine serum (FBS), Hank's balanced salt solution (HBSS), phosphate-buffered saline (PBS), and tris−acetate EDTA (TAE) were purchased from Thermo Fisher Scientific. Milli-Q-grade purified water was obtained from a Milli-Q UV purification system (Sartorius Stedim Biotech S.A., Aubagne Cedex, France). 2′,7′-Dichlorodihydrofluorescein diacetate and Cremophor EL were purchased from Sigma-Aldrich, Mitotracker Red CMXRos was purchased from Molecular Probes, Eugene, OR, USA, and Hoechst 33342 was purchased from B.D. Bioscience, San Jose, CA, USA, accordingly. DNA extraction and purification kits were obtained from QIAgen, Germany.

Instrumentation. ^1H and ^{13}C NMR spectra were recorded using Varian (Agilent, USA) 400 and 100 MHz NMR spectrometers equipped with a 5 mm ATB probe. The chemical shifts, δ, were reported in ppm (parts per million), and coupling constants were reported in Hertz. The residual solvent peaks were used as an internal reference. The abbreviations for the peak multiplicities are as follows: s (singlet), d (doublet), dd (doublet of doublets), t (triplet), q (quartet), m (multiplet), and br (broad). Elemental analysis was carried out with the addition of V_2O_5 using an Elemental MicroCube CHN analyzer. Infrared spectra were recorded on a Nicolet 6700 FT-IR spectrometer using the ATR technique. ESI mass spectra measurements of complexes were carried out on a high-resolution mass spectrometer (Sciex X500R Q-TOF). Cell viability assay was performed using the BioTek Synergy H1 microplate reader. Confocal microscopy was performed using a Leica Confocal SP8 Microscope (Super Resolution). Agarose gel imaging was performed under UV light using a ChemiDoc Touch Imaging System (BioRad). The DNA concentrations were quantified using a NanoDrop One/OneC Microvolume UV−Vis spectrophotometer.

Synthesis. General Procedure for Ligand Synthesis. All ligands were synthesized according to a literature procedure using a condensation reaction between 1,10-phenathroline-5,6-dione and diamine.[31] The characterization of the ligands was in agreement with the literature data.[32−34]

General Procedure for the Synthesis of Ru Complexes. The solution of $[(\eta^6\text{-arene})RuCl_2]_2$ (1 eq) in methanol (5 mL) was added to a solution of its respective ligand (2 eq) in a methanol/CH_2Cl_2 mixture (10 mL) 1/1 (v/v). The mixture was stirred at room temperature for 5 h. NH_4PF_6 (3 eq) was then added to the solution and left to stir overnight. The formed yellow precipitate was filtered and washed with cold MeOH and Et_2O and dried in vacuo.

Synthesis of $[(\eta^6\text{-Benzene})Ru(Medppz)Cl]PF_6{\cdot}H_2O$ (1A). $[(\eta^6\text{-Benzene})RuCl_2]_2$ (precursor **1**) (50 mg, 0.099 mmol, 1 eq.), Medppz (ligand **A**) (59 mg, 0.199 mmol, 2 eq.), and NH_4PF_6 (48 mg, 0.297 mmol, 3 eq.). Yield: 110 mg (82%). Calcd. for: $C_{25}H_{20}ClF_6N_4PRuO$ C 44.55; H 2.99; N 8.31. Found: C 44.92; H 2.83; N 8.61. IR (cm^{-1}): 3091, 1608 (C═N), 1501, 1414, 1357, 837, 557. ^1H NMR (400 MHz, DMSO-d_6): δ 10.07 (d, J = 5.2 Hz, 2H), 9.39 (dd, J = 14.3, 8.1 Hz, 2H), 8.26−8.16 (m, 2H), 8.00 (d, J = 8.6 Hz, 1H), 7.92 (s, 1H), 7.76 (d, J = 8.7 Hz, 1H), 6.35 (s, 6H), 2.56 (s, 3H). $^{13}C\{^1H\}$ NMR (101 MHz, DMSO-d_6): δ 157.96, 157.85, 150.58, 148.18, 148.01, 143.78, 142.18, 140.75, 138.86, 138.20, 135.47, 135.42, 135.34,

https://doi.org/10.1021/acs.inorgchem.3c00570
Inorg. Chem. 2023, 62, 8188−8199

129.62, 129.55, 129.12, 127.92, 127.75, 87.33, 22.06. ESI-HRMS: $[M\text{-}PF_6]^+$: 511.0429 (calculated 511.02634).

*Synthesis of [(η^6-Toluene)Ru(Medppz)Cl]PF_6 (**2A**).* [(η^6-Toluene)-$RuCl_2]_2$ (precursor **2**) (50 mg, 0.095 mmol, 1 eq), Medppz (ligand **A**) (56 mg, 0.189 mmol, 2 eq), and NH_4PF_6 (46 mg, 0.285 mmol, 3 eq). Yield: 124 mg (94%). Calcd. for: $C_{26}H_{20}ClF_6N_4PRu$ C 46.61; H 3.01; N 8.36. Found: C 46.23; H 2.92; N 8.60. IR (cm^{-1}): 3073, 1578 (C═N), 1500, 1413, 1357, 840, 558. ^1H NMR (400 MHz, DMSO-d_6): δ 9.96 (d, J = 5.1 Hz, 4H), 9.35 (dd, J = 15.8, 8.2 Hz, 4H), 8.25−8.14 (m, 4H), 7.94 (d, J = 8.7 Hz, 2H), 7.87 (s, 2H), 7.72 (d, J = 8.7 Hz, 2H), 6.45 (t, J = 5.7 Hz, 4H), 6.09 (d, J = 6.0 Hz, 4H), 5.90 (t, J = 5.6 Hz, 2H), 2.53 (s, 5H), 2.29 (s, 5H). $^{13}C\{^1H\}$ NMR (101 MHz, DMSO-d_6): δ 162.27, 157.74, 157.63, 150.58, 148.24, 148.07, 143.76, 142.10, 140.66, 138.82, 138.17, 135.37, 135.32, 129.51, 129.44, 129.06, 127.86, 127.81, 127.76, 106.24, 90.54, 83.40, 80.64, 22.04, 19.32. ESI-HRMS: $[M\text{-}PF_6]^+$: 525.0560 (calculated 525.04199).

*Synthesis of [(η^6-Cymene)Ru(Medppz)Cl]PF_6 (**3A**).* [(η^6-Cymene)-$RuCl_2]_2$ (precursor **3**) (50 mg, 0.079 mmol, 1 eq), Medppz (ligand **A**) (40 mg, 0.158 mmol, 2 eq), NH_4PF_6 (38 mg, 0.237 mmol, 3 eq). Yield: 81 mg (72%). Calcd. for: $C_{29}H_{26}ClF_6N_4PRu$ C 48.92; H 3.68; N 7.87. Found: C 48.75; H 3.59; N 8.29. IR (cm^{-1}): 3132, 3047, 2877, 1607 (C═N), 1498, 1411, 1357, 845, 558. ^1H NMR (400 MHz, DMSO-d_6): δ 9.96 (s, 2H), 9.54 (t, J = 7.8 Hz, 2H), 8.29−8.21 (m, 2H), 8.15 (d, J = 8.6 Hz, 1H), 8.06 (s, 1H), 7.86 (d, J = 8.8 Hz, 1H), 6.35 (d, J = 6.1 Hz, 2H), 6.12 (d, J = 6.1 Hz, 2H), 2.74−2.57 (m, 4H), 2.18 (s, 3H), 0.96 (d, J = 6.8 Hz, 6H). $^{13}C\{^1H\}$ NMR (101 MHz, DMSO-d_6): δ 162.22, 157.63, 150.58, 148.25, 148.08, 143.80, 142.35, 140.94, 139.31, 138.65, 135.48, 129.84, 129.79, 129.23, 128.03, 127.96, 105.23, 103.13, 86.34, 84.65, 30.88, 22.18, 22.09, 18.66. ESI-HRMS: $[M\text{-}PF_6]^+$: 567.1046 (calculated 567.08894).

*Synthesis of [(η^6-Benzene)Ru(NO_2dppz)Cl]PF_6 (**1B**).* [(η^6-Benzene)$RuCl_2]_2$ (precursor **1**) (46 mg, 0.092 mmol, 1 eq); NO_2dppz (ligand **B**) (60 mg, 0.183 mmol, 2 eq), NH_4PF_6 (45 mg, 0.275 mmol, 3 eq). Yield: 114 mg (90%). Calcd. for: $C_{24}H_{15}ClF_6N_5O_2PRu$ C 41.97; H 2.20; N 10.20. Found: C 42.30; H 2.26; N 10.11. IR (cm^{-1}): 3092, 1732, 1611 (C═N), 1526 (NO_2), 1352 (NO_2), 1053, 833, 729, 556. ^1H NMR (400 MHz, DMSO-d_6): δ 10.12 (s, 2H), 9.66 (d, J = 5.5 Hz, 2H), 9.18 (s, 1H), 8.73 (d, J = 8.7 Hz, 1H), 8.61 (d, J = 9.2 Hz, 1H), 8.29 (s, 2H), 6.35 (s, 6H). $^{13}C\{^1H\}$ NMR (101 MHz, DMSO-d_6): δ 160.91, 158.90, 158.74, 149.21, 149.15, 148.94, 144.12, 142.06, 141.58, 140.96, 136.37, 136.10, 131.92, 129.47, 129.42, 128.25, 125.92, 125.66, 87.44. ESI-HRMS: $[M\text{-}PF_6]^+$: 542.0118 (calculated 541.99578).

*Synthesis of [(η^6-Toluene)Ru(NO_2dppz)Cl]PF_6 (**2B**).* [(η^6-Toluene)$RuCl_2]_2$ (precursor **2**) (50 mg, 0.094 mmol, 1 eq); NO_2dppz (ligand **B**) (62 mg, 0.188 mmol, 2 eq); NH_4PF_6 (46 mg, 0.282 mmol, 3 eq) Yield: 128 mg (97%). Calcd. for: $C_{25}H_{17}ClF_6N_5O_2PRu$ C 42.84; H 2.44; N 9.99. Found: C 42.42; H 2.66; N 9.79. IR (cm^{-1}): 3093, 1610 (C═N), 1529 (NO_2), 1354 (NO_2), 1499, 1419, 1354, 839, 729, 558. ^1H NMR (400 MHz, DMSO-d_6): δ 10.04 (d, J = 5.3 Hz, 2H), 9.64 (dd, J = 8.1, 3.0 Hz, 2H), 9.18 (d, J = 2.2 Hz, 1H), 8.72 (dd, J = 9.3, 2.3 Hz, 1H), 8.60 (d, J = 9.3 Hz, 1H), 8.29 (dt, J = 8.3, 5.1 Hz, 2H), 6.47 (t, J = 5.9 Hz, 2H), 6.10 (d, J = 6.1 Hz, 2H), 5.90 (t, J = 5.6 Hz, 1H), 2.28 (s, 3H). $^{13}C\{^1H\}$ NMR (101 MHz, DMSO-d_6): δ 158.66, 158.51, 149.27, 149.14, 149.00, 144.10, 142.10, 141.63, 140.94, 136.23, 135.94, 131.88, 129.38, 129.33, 128.23, 128.18, 125.90, 125.62, 106.26, 90.56, 83.47, 80.84, 19.31. ESI-HRMS: $[M\text{-}PF_6]^+$: 556.0288 (calculated 556.01143).

*Synthesis of [(η^6-Benzene)Ru(CO_2Medppz)Cl]PF_6 (**1C**).* [(η^6-Benzene)$RuCl_2]_2$ (precursor **1**) (65 mg, 0.129 mmol, 1 eq), CO_2Medppz (ligand **C**) (88 mg, 0.259 mmol, 2 eq), NH_4PF_6 (64 mg, 0.389 mmol, 3 eq). Yield: 157 mg (86%). Elemental analysis: Calcd. for: $C_{26}H_{18}ClF_6N_4O_2PRu$ C 44.62; H 2.59; N 8.00. Found: C 44.58; H 2.66; N 7.83. IR (cm^{-1}): 3091, 1731 (C═O), 1627 (C═N), 1256, 1092, 836, 558. ^1H NMR (400 MHz, DMSO-d_6): δ 10.10 (t, J = 4.1 Hz, 4H), 9.55 (dd, J = 7.8, 3.6 Hz, 4H), 8.79 (d, J = 1.0 Hz, 2H), 8.38 (dt, J = 16.5, 5.2 Hz, 4H), 8.30−8.23 (m, 4H), 6.36 (s, 11H), 3.99 (s, 6H). $^{13}C\{^1H\}$ NMR (101 MHz, DMSO-d_6): δ 165.57, 158.54, 158.40, 150.51, 150.50, 148.85, 148.62, 143.70, 141.34, 140.98, 140.47, 136.06, 135.85, 132.79, 131.72, 131.09, 130.54, 129.49, 128.04, 87.36, 53.46. ESI-HRMS: $[M\text{-}PF_6]^+$: 555.0353 (calculated 555.01618).

*Synthesis of [(η^6-Toluene)Ru(CO_2Medppz)Cl]PF_6 (**2C**).* [(η^6-Toluene)$RuCl_2]_2$ (precursor **2**) (68,5 mg, 0.129 mmol, 1 eq), CO_2Medppz (ligand **C**) (88 mg, 0.258 mmol, 2 eq), NH_4PF_6 (63 mg, 0.387 mmol, 3 eq). Yield: 170 mg (92%). Calcd. for: $C_{27}H_{20}ClF_6N_4O_2PRu$ C 45.42; H 2.82; N 7.85. Found: C 45.28; H 2.85; N 7.57. IR (cm^{-1}): 3078, 1731 (C═O), 1626 (C═N), 1448, 1254, 1091, 837, 730, 558. ^1H NMR (400 MHz, DMSO-d_6): δ 10.09−9.98 (m, 2H), 9.53 (dd, J = 8.0, 4.0 Hz, 2H), 8.77 (s, 1H), 8.36 (dt, J = 18.4, 5.2 Hz, 2H), 8.28−8.22 (m, 2H), 6.47 (t, J = 5.9 Hz, 2H), 6.11 (d, J = 6.1 Hz, 2H), 5.92 (t, J = 5.7 Hz, 1H), 3.99 (s, 3H), 2.29 (s, 3H). $^{13}C\{^1H\}$ NMR (101 MHz, DMSO-d_6): δ 165.56, 161.69, 158.40, 158.25, 150.51, 148.91, 148.69, 143.66, 141.30, 141.00, 140.49, 135.95, 135.74, 132.77, 131.70, 131.06, 130.52, 129.39, 128.06, 106.26, 90.56, 83.47, 80.80, 53.45, 19.33. ESI-HRMS: $[M\text{-}PF_6]^+$: 569.0451 (calculated 569.03183).

*Synthesis of [(η^6-Cymene)Ru(CO_2Medppz)Cl]$PF_6 \cdot H_2O$ (**3C**).* [(η^6-cymene)$RuCl_2]_2$ (precursor **3**) (74 mg, 0.12 mmol, 1 eq), CO_2Medppz (ligand **C**) (82 mg, 0.241 mmol, 2 eq), NH_4PF_6 (59 mg, 0.361 mmol, 3 eq). Yield: 165 mg (88%). Calcd. for: $C_{30}H_{28}ClF_6N_4O_3PRu$ C 46.55; H 3.65; N 7.24. Found: C 45.99; H 3.68; N 7.84. IR (cm^{-1}): 3056, 2973, 1727 (C═O), 1624 (C═N), 1415, 1320, 840, 773, 558. ^1H NMR (400 MHz, DMSO-d_6): δ 10.02 (d, J = 4.7 Hz, 2H), 9.60 (d, J = 8.1 Hz, 2H), 8.83 (s, 1H), 8.47−8.36 (m, 2H), 8.33−8.21 (m, 2H), 7.16 (s, 2H), 6.38 (d, J = 6.4 Hz, 2H), 6.15 (d, J = 6.4 Hz, 2H), 3.98 (s, 3H), 2.67 (dt, J = 13.8, 6.9 Hz, 1H), 2.19 (s, 3H), 0.97 (d, J = 6.9 Hz, 5H). $^{13}C\{^1H\}$ NMR (101 MHz, DMSO-d_6): δ 165.62, 148.84, 148.61, 143.73, 141.35, 141.28, 140.77, 135.81, 132.81, 131.72, 130.57, 129.60, 128.20, 105.31, 86.37, 84.67, 53.44, 30.88, 22.20, 18.69. ESI-HRMS: $[M\text{-}PF_6]^+$: 611.0967 (calculated 611.07878).

Cyclic Voltammetry. Electrochemical measurements were conducted in a three-electrode cell (volume of 5 mL), where glassy carbon electrode (3 mm diameter) was used as a working electrode, Ag/AgCl (3 M KCl) was used as a reference electrode, and platinum wire was used as a counter electrode. The concentration of the Ru complexes was 1 mg/mL in DMSO containing 0.1 M tetrabutylammonium perchlorate as the supporting electrolyte. Measurements were carried out in a potential range from −0.8 to 1.5 V at a scan rate of 50 mV/s using a CHI instrument model 760b (Austin, Texas, USA).

Stability Studies. To check the stability of **1A**−**3A**, **1B**, **2B**, and **1C**−**3C** in DMSO, these compounds were dissolved in DMSO-d_6, and ^1H NMR spectra were obtained at 0, 24, 48 and 72 h timepoints. For stability studies, all compounds were dissolved in 1% DMSO in PBS or complete colorless cell culture media (DMEM containing 10% FBS and 1% penicillin−streptomycin)/H_2O (1:9) solvent system. All solutions were kept at 37 °C throughout the experiment. The UV−Vis profiles of the samples were recorded at 0, 24, and 72 h using a Cary 50 spectrophotometer (Varian) with the following parameters: start wavelength = 200 nm, end wavelength = 800 nm, scan speed = 400 nm/min, sampling interval = 0.5, slit width = 1.5, and path length = 10. Blank calibration and baseline correction were performed before every measurement. Quartz cuvettes have been used for the measurement of original samples.

Cell Lines and Culture Conditions. Human cancer cell lines HCT116 (human colorectal carcinoma), CT26 (murine colorectal adenocarcinoma), MDA-MB-231 (human breast adenocarcinoma), and MRC5 (human lung fibroblasts, non-cancerous) were obtained from ATCC. HCT116, MDA-MB-231, CT26, and MRC5 were cultured in DMEM containing 10% FBS and 1% penicillin−streptomycin (10,000 U/mL). Cells were grown in tissue culture flasks (75 cm^2 and 25 cm^2, SPL Life Sciences). All cell lines were grown at 37 °C in a humidified atmosphere of 95% air and 5% CO_2. All drug stock solutions were prepared in DMSO, and the final concentration in the medium did not exceed 1%, at which cell viability was not inhibited.

Cell Viability Assay. The cytotoxicity of compounds was determined using an MTT colorimetric test. The cells were harvested

https://doi.org/10.1021/acs.inorgchem.3c00570
Inorg. Chem. 2023, 62, 8188−8199

from culture flasks by trypsinization and seeded into Cellstar 96-well microculture plates at the seeding density of 6000 cells per well (6×10^4 cells/mL). After the cells were allowed to resume exponential growth for 24 h, they were exposed to drugs at different concentrations in media for 72 h. The drugs were diluted in complete medium at the desired concentration and added to each well (100 μL) and serially diluted to other wells. After exposure for 72 h, the media was replaced with MTT in media (5 mg/mL, 100 μL/well) and incubated for an additional 50 min. Subsequently, the medium was aspirated, and the purple formazan crystals formed in viable cells were dissolved in DMSO (100 μL/well). Optical densities were measured at 570 nm using a BioTek Synergy H1 microplate reader. The quantity of viable cells was expressed in terms of treated/control (T/C) values in comparison to untreated control cells, and 50% inhibitory concentrations (IC_{50}) were calculated from concentration−effect curves by interpolation. Evaluation was based on means from at least three independent experiments, each comprising three replicates per concentration level.

ROS Detection via Confocal Microscopy. HCT116 cells were seeded onto 4-well chamber slides with removable wells (Nunc Lab-Tek II Chamber Slide System) at a 1×10^5/mL density (1 mL per well). Cells were allowed to resume exponential growth for 24 h. The cell culture medium was aspirated and washed with PBS (2×). In a low-light environment, the H_2DCFDA (2′,7′-dichlorodihydrofluorescein diacetate) solution prepared in 1× HBSS (20 μM, 1 mL) was added to each well and incubated for 30 min (37 °C, 5% CO2). DCFDA solution was removed and washed with HBSS (2×500 μL). The drug solutions at desired concentrations were prepared in colorless, serum-free cell culture media and added to the cells, and then the chamber slides were incubated for 4 h (37 °C, 5% CO_2). After that, the drug-containing media was removed and the wells were washed with PBS (2×500 μL). Then, the cells were incubated with a culture medium containing 1 μM Mitotracker Red CMXRos and 10 μg/mL Hoechst 33342 for 15 min. After that, the cells were washed with PBS (2×500 μL) and mounted on a slide with mounting media glycerol:PBS (9:1). The samples were protected from photodegradation by covering them with aluminum foil before imaging. Images were acquired using a Leica confocal laser scanning microscope and analyzed via Microscope Software Platform LAS X Life Science.

Quantitative ROS Detection via Flow Cytometry. HCT116 cells were seeded onto 6-well plates at a 3×10^5 cells/mL density (2 mL per well). Cells were allowed to resume exponential growth for 24 h. The cell culture medium was aspirated and washed with PBS (1×). The drug solutions at desired concentrations were added to the cells and incubated for 4 h (37 °C, 5% CO_2). Subsequently, the drug-containing media was removed, and the wells were washed with PBS (2×500 μL). Afterward, the cells were trypsinized, normalized to 1×10^6 cells/mL, transferred to microcentrifuge tubes, washed, and centrifuged to eliminate the supernatant. After centrifugation, the cells were resuspended in a colorless medium (FBS and phenol red-free) containing H_2DCFDA (20 μM) and incubated for 30 min (37 °C, 5% CO_2). Next, the H_2DCFDA solution was removed, and the cells were washed and resuspended in PBS. Immediately before analyzing by flow cytometry, the cells were stained with propidium iodide (PI, 100 μg/mL) to exclude necrotic cells and subsequently protected from photodegradation with aluminum foil. A cytometer by Beckman Coulter (CytoFLEX) was used to evaluate the distribution of the DCF-stained cells. FlowJo software (ver. 10.8.1) was used for the analysis of flow cytometry data.

DNA Degradation Assay. HCT116 cells were seeded onto 6-well plates (Greiner Bio-One) at a density of 3×10^5 cells/mL (2 mL per well). The cells were allowed to resume exponential growth for 24 h. The cell culture medium was aspirated and washed with PBS (2×1 mL) and replaced with compounds at the respective $IC_{50\ (72h)}$ concentrations in DMEM for 24 h at 37 °C and 5% CO_2. DNA extraction and purification were done based on the manufacturer's instructions (QIAgen DNA Extraction and Purification Kit). The DNA concentrations were normalized using a NanoDrop One/OneC Microvolume UV−Vis spectrophotometer. The normalized DNA samples were loaded onto 1% agarose gel and subjected to electrophoresis for 2 h at 80 V in a TAE running buffer (tris−acetate EDTA). The gels were photographed under UV light using a ChemiDoc Touch Imaging System (BioRad). The digital images were analyzed using BioRad Image Lab Software.

In Vivo Studies. All animal procedures were performed under the Guidelines for Care and Use of Laboratory Animals of the City University of Hong Kong and approved by the Animal Ethics Committee of the City University of Hong Kong. All mice were maintained in the laboratory animal research unit (LARU) of the City University of Hong Kong in specific pathogen-free conditions. All mice experiments were performed in compliance with the guidelines and protocols approved by the institutional and local ethics committee of HKSAR, Department of Health. Six- to eight-week-old BALB/c mice were purchased from the Laboratory Animal Research Unit (LARU) of the City University of Hong Kong. Animals were randomly assigned to different groups. Prior to assignment to groups, the weight variation of the animals did not exceed 20% of the mean weight. Animals were grouped and housed in solid bottom polycarbonate cages (5 mice per cage) and provided with pelleted food and water ad libitum. Environmental controls for the animal room were set to maintain 22−27 °C, a relative humidity of 55−75%, a minimum of 10 air changes/h, and a 12 h light/12 h dark cycle. No known contaminants were present in the diet or water at levels that might interfere with this study. To identify the appropriate dose of the experimental drugs for subsequent in vivo efficacy studies, BALB/c mice were injected every second day via the i.p. route with 20 mg/kg of Ru complex **3A** or 0.8 mg/kg of ligand **A** for 6 days (3 injections in total). Subsequently, the mice were monitored for 5 more days. The control group received only the respective vehicle (DMSO/Cremophor EL/PBS). The location of the i.p. injection was the lower left abdominal quadrant. Animals were controlled for distress development. Their weight changes were monitored every second day for 2 weeks. On day 6, two mice receiving 20 mg/kg of **3A** died; therefore, another group of mice was treated with 8 mg/kg of **3A** using the similar regimen. Mice receiving 8 mg/kg of **3A**, 0.8 mg/kg of **A**, or a vehicle did not show any signs of toxicity. For in vivo efficacy studies, BALB/c mice were subcutaneously injected with 0.1 mL of CT26 cells (5×10^6 cells/L) on the right flank. After the tumors became palpable (day 10 after implantation), treatment was initiated. Animals were randomly divided into three groups ($n = 5$), and the tumor dimensions were measured using a caliper. The volume (mm^3) of the tumor was calculated according to the formula tumor volume = (longest diameter) × (shortest diameter)^2 × 0.5. Drug-treated groups were injected with 8 mg/kg **3A** or 0.8 mg/kg **A** in sterile PBS with DMSO/Cremophor EL, whereas the control group was injected with sterile PBS with DMSO/Cremophor EL as a vehicle. Treatment was performed on days 10, 12, 14, 16, and 18. After the end of treatment, animals were sacrificed on day 21. Animals were controlled for distress development. Their weight changes were monitored every day for 3 weeks. All mice were bright, alert, and responsive during the whole study. After sacrificing the mice, the tumors were collected, weighed, and together with the organs (liver and kidney) were harvested for further histopathological examination.

Histopathological Analysis. Tumor, liver, and kidney tissues were fixed in 10% buffered formalin overnight and washed twice with PBS. The tissues were then embedded in paraffin. Sections with thicknesses of 4 μm were prepared, mounted on slides, and deparaffinized in xylene (twice). Then, the sections were rehydrated in a graded series of alcohol ($2 \times 100\%$ alcohol and $2 \times 75\%$ alcohol) and distilled water. Later, the sections were stained with a hematoxylin solution, rinsed in water, passed through a 70% ethanol solution containing 1% HCl, and rinsed again with tap water. The sections were stained with eosin for 5 min and rinsed with absolute alcohol and xylene for 5 min.[35] The slides were analyzed using a Leica DM2700 microscope and a Panoramic 250 Flash III (3D Histech, Hungary). Necrosis, hemorrhages, steatosis in hepatocytes, cell shrinking, nuclear enlargement or pyknosis, chromatin condensation, ruptured cell membranes, and apoptotic bodies were evaluated as potential signs of liver and kidney toxicity.[36] The extent of tumor

https://doi.org/10.1021/acs.inorgchem.3c00570
Inorg. Chem. 2023, 62, 8188−8199

Scheme 1. Synthetic Route toward Complexes 1A−3A, 1B, 2B, and 1C−3C with the Numbering Scheme Used for the NMR Assignment

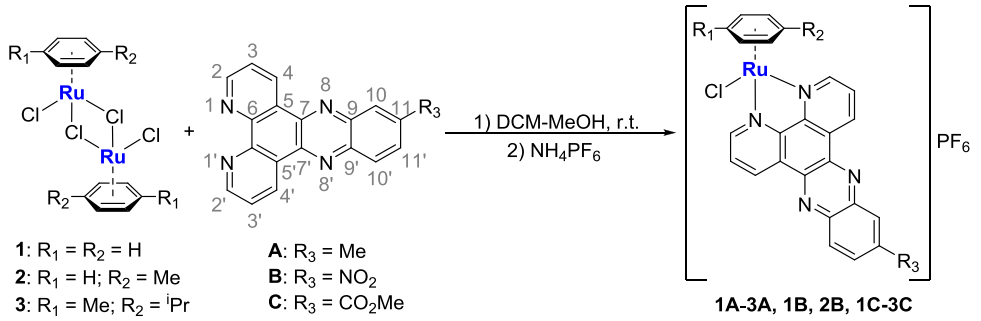

necrosis was quantified on H&E-stained slides by evaluating the percent of tumor necrotic area by the visual assessment of an experienced pathologist.

Statistical Analysis. Quantitative data are presented as means ± SD from at least three independent experiments. For the in vivo data, the significance of the differences was evaluated with two-way ANOVA followed by Tukey's multiple comparison post-test. Statistical analysis was executed with GraphPad Prism Software (San Diego, CA, USA) using $p < 0.05$ as the critical significance level.

RESULTS AND DISCUSSION

Synthesis and Characterization. Ru complexes **1A−3A**, **1B**, **2B**, and **1C−3C** were synthesized following the synthetic route described in Scheme 1. 11-Methyldipyrido[3,2-*a*:2′,3′-*c*]phenazine (**A**), 11-nitrodipyrido[3,2-*a*:2′,3′-*c*]phenazine (**B**), and methyl dipyrido[3,2-*a*:2′,3′-*c*]phenazine-11-carboxylate (**C**) were used as ligands. They were prepared using a standard method based on the Schiff base condensation of 1,10-phenanthroline-5,6-dione with the respective diamine. The subsequent complexation of 2 eq of dppz ligands **A−C** with 1 eq of the corresponding (arene)Ru dimers in methanol yielded complexes **1A−3A**, **1B**, **2B**, and **1C−3C** in moderate to almost quantitative yields. They were found to be soluble in DMSO, methanol, and acetonitrile. All complexes were characterized by high-resolution mass-spectrometry (Figures S1−S8), ^{1}H NMR, and ^{13}C NMR spectroscopy (Figures S9−S24), and their purity was confirmed by elemental analysis.

The identity of the complexes was verified by high-resolution mass spectrometry, and their purity was confirmed by elemental analysis. The mass spectra of all the complexes revealed high-intensity signals corresponding to M^{+} ions. The observed isotopic distribution pattern was in good agreement with the calculated mass distribution. Analysis of the NMR spectra revealed that the chemical shifts of the protons and carbons of the Ru complexes were in agreement with the previously published structurally similar compounds.[21,25] As expected, the arene-to-ligand ratio was found to be 1:1 as determined by the integration of protons in the ^{1}H NMR spectra. The six protons originated from the benzene moiety in complexes **1A−1C** were located at 6.35 ppm. The signals from the toluene moiety in complexes **2A−2C** were present at ca. 6.46, 6.10, and 5.91 ppm, whereas the methyl group was detected at 2.45 ppm. The signals from the cymene moiety in complexes **3A** and **3C** were located at ca. 6.36 and 6.13 ppm; the signals from one methyl group and two other methyl groups were at 2.18 and 0.96 ppm, respectively, while the signal from the isopropyl group was located at 2.65 ppm.

The coordination of ligands **A−C** to the (arene)Ru fragments resulted in the significant downfield shift of the protons in complexes, which were located in the *ortho* and *meta* positions to the nitrogen in the phen fragment. On the other hand, the protons in the *para* position as well as the phenazine protons remained largely unaffected. Similar observations were previously reported for other Ru-dppz complexes.[21] For example, in the uncoordinated ligand **A**, the signals of H2(H2′) and H4(H4′) protons appeared at 9.47 and 9.16 ppm, respectively. Upon coordination to the (arene)Ru moiety, the signals of H2(H2′) and H4(H4′) protons shifted to 10.07 and 9.39 ppm, respectively. A similar downfield shift occurred for the signal of H3(H3′) protons, which shifted from 7.90 ppm in the uncoordinated ligand **A** to 8.20 ppm. Atoms H10, H11, and H11′ were less affected by the coordination and displayed a slight upfield shift in comparison with uncoordinated ligand **A**. Ligand **B** showed less pronounced proton shifts upon coordination to the Ru center. Protons H2(H2′) displayed an upfield shift from 10.15 ppm in the uncoordinated ligand **B** to 10.11 and 10.04 ppm in complexes **1B** and **2B**, respectively. The signal of H4(H4′) shifted downfield from 9.55 ppm in the uncoordinated ligand **B** to 9.64 ppm in **1B** and **2B**. The most significant shift was observed for ligand **C** and complex **1C**. Ligand protons H2(H2′) and H4(H4′) shifted from 9.29 and 9.15 ppm in the uncoordinated ligand **C** to 10.10 and 9.55 ppm in complex **1C**, respectively. In complexes **2C** and **3C**, these protons were located at 10.02 and 9.55 ppm, respectively. Proton signals originated from H3(H3′) atoms were also shifted downfield from 7.64 ppm in the uncoordinated ligand **C** to 8.27 ppm in **1C−3C**. The downfield shift for the protons that were located further from the Ru center, such as H10, H11, and H11′, was less significant (around 0.2−0.3 ppm).

In ^{13}C{^{1}H} NMR spectra, the signals from the arene moieties appeared at usual values for this type of piano-stool complexes.[21,25] For example, ^{13}C signals from the benzene moiety were located at 87.4 ppm in complexes **1A**, **1B**, and **1C**. ^{13}C signals from the toluene moiety in complexes **2A**, **2B**, and **2C** appeared at 106.2, 90.5, 83.4, and 80.6 ppm, while a methyl group was located at 19.3 ppm. ^{13}C signals from the cymene moiety were present at 105.2, 103.1, 86.3, and 84.6 ppm, while a methyl group was located at 18.6 ppm. ^{13}C signals from the isopropyl group were located at 30.8 ppm (CH) and 22.2 ppm (CH_3). ^{13}C signals of the C2 and C3 atoms of the dppz ligands were mostly affected by the coordination to the Ru center. Whereas in the uncoordinated ligands, C2 signals were located at ca. 152 ppm, in **1A−3A**, these signals were shifted downfield to ca. 157.5 ppm, in **1B** and **2B** to ca. 158.6 ppm, and in **1C−3C** to ca. 158.2 ppm. The C3 signals in the uncoordinated ligands were present at 133.6 ppm, and in all complexes, they

https://doi.org/10.1021/acs.inorgchem.3c00570
Inorg. Chem. 2023, 62, 8188−8199

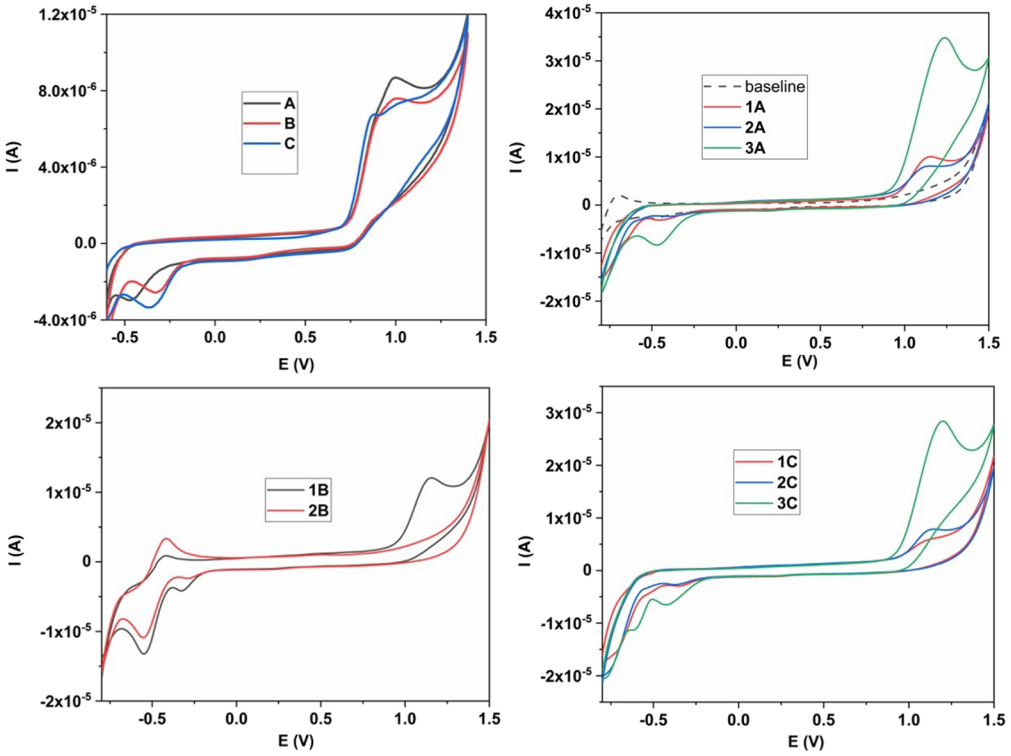

Figure 1. Cyclic voltammograms of dppz ligands **A**–**C** and Ru-dppz complexes **1A**–**3A**, **1B**, **2B**, and **1C**–**3C** in DMSO/*n*-Bu_4NClO_4 with a glassy carbon working electrode at a scan rate of 50 mV s^{-1}.

were shifted downfield to 136.2–135.3 ppm. The ^{13}C signals of other atoms in the coordinated dppz ligands were less affected by the coordination.

The IR spectrum of the ligand **A** exhibited a very strong band at 1586 cm^{-1} due to the C═N stretching. In complexes **1A**, **2A**, and **3A** characteristic bands at 1608, 1578, and 1607 cm^{-1} from pyridine ν(C═N) showed a downward and upward shift in comparison with the uncoordinated ligand. The C═N stretching in the ligand **B** was observed at 1618 cm^{-1}, and it was shifted to 1611 and 1610 cm^{-1} in **1B** and **2B**, respectively. An asymmetric stretch from the nitro group in the ligand **B** was observed at 1521 cm^{-1}, and in complexes **1B** and **2B**, it was observed at 1526 and 1529 cm^{-1}, respectively. The symmetric stretch of the nitro group also showed a downward shift from 1343 cm^{-1} in the uncoordinated ligand **B** to 1352 and 1354 cm^{-1} in complexes **1B** and **2B**, respectively. The pyridine ν(C═N) stretch band was shifted from 1621 cm^{-1} in the uncoordinated ligand **C** to 1627, 1626, and 1624 cm^{-1} in complexes **1C**, **2C**, and **3C**, respectively. The ν(C═O) stretch in the uncoordinated ligand **C** was observed at 1737 cm^{-1} and was shifted to 1731, 1731, and 1727 cm^{-1} in the corresponding complexes **1C**, **2C**, and **3C**, respectively.

Electrochemistry. Electrochemical measurements of the ligands and their respective Ru complexes were carried out in tetrabutylammonium phosphate supporting electrolyte at scan rate of 50 mV s^{-1} (Figure 1), and the electrochemical potentials are summarized in Table S1. In the case of the methyl-substituted dppz ligand **A**, only one reduction can be observed (E^1_{red} = −0.47 V with respect to Ag/AgCl reference electrode). The nitro-substituted dppz ligand **B** and methoxycarbonyl-substituted dppz ligand **C** showed two reduction processes (E^1_{red} = −0.30 V and E^2_{red} = −0.37 V for **B** and E^1_{red} = −0.28 V and E^2_{red} = −0.33 V for **C** with respect to the Ag/AgCl reference electrode). As can be seen, the substitution of the methyl group with -NO_2 or -COOMe groups resulted in less negative redox potentials. Thus, ligands **B** and **C** are easier to reduce, as expected upon the introduction of the electron-withdrawing substituents, leading to the decrease of the electron density within the dppz ligand. Similar observations were reported in the literature for structurally similar dppz ligands.[37]

The electrochemical behavior of the corresponding Ru complexes was more complex. Briefly, in the positive region of the cyclic voltammograms, all complexes with the exception of **2B** displayed one irreversible redox peak between 1.12 and 1.29 V, corresponding to Ru^{2+}/Ru^{3+} oxidation. In contrast, the negative region of the cyclic voltammograms of the Ru-dppz complexes was less well-defined. Complexes **1A**–**3A** with a Me-substituted dppz ligand displayed one irreversible reduction (E^1_{red} = −0.45, −0.38, and − 0.47 V for **1A**, **2A**, and **3A**, respectively, with respect to the Ag/AgCl reference electrode). On the contrary, the cyclic voltammograms of complexes **1B** and **2B** with a NO_2-substituted dppz ligand displayed the first irreversible reduction peak at E^1_{red} = −0.33 and −0.29 V for **1B** and **2B**, respectively, and the second reversible reduction peak at E^1_{red} = −0.55 V for **1B** and **2B** with respect to the Ag/AgCl reference electrode. The reduction processes in complexes **1C**–**3C** seemed to be irreversible with E^1_{red} = −0.35, −0.36, and −0.43 V for **1C**, **2C**, and **3C**, respectively, with respect to the Ag/AgCl reference electrode. Additionally, the cyclic voltammogram of **3C** was characterized by the very defined second irreversible reduction peak at E^2_{red} = −0.61 V. The observed electrochemical behavior of the dppz ligands and (arene)Ru-dppz complexes indicates that all tested compounds might be electrochemically active in the cells, leading to the induction of ROS; however, they are not expected to undergo reversible redox cycling unlike other metal complexes, which generate ROS via Fenton-like chemistry.[38]

https://doi.org/10.1021/acs.inorgchem.3c00570
Inorg. Chem. 2023, 62, 8188−8199

Table 1. Cytotoxicity of dppz Ligands and Corresponding Half-Sandwich Ru Complexes Determined by the MTT Assay after 72 h of Exposure

		IC_{50} (μM)[a]					
type	compound	MDA-MB-231	HCT116	CT26	MRC5	SF_{MDA}[b]	SF_{HCT116}[c]
ligand	**A** (-Me)	2.0 ± 0.3	1.3 ± 0.2	2.5 ± 1.0	13 ± 4	6	10
	B (-NO_2)	1.8 ± 0.6	1.1 ± 0.2	1.1 ± 0.4	2.2 ± 0.9	1	2
	C (-CO_2Me)	>2[d]	>2	>2	>2		
Ru complex	**1A**	35 ± 7	81 ± 15	166 ± 57	178 ± 24	5	2
	2A	23 ± 8	27 ± 5	168 ± 19	121 ± 40	5	5
	3A	2.0 ± 0.6	2.1 ± 0.2	12 ± 2.0	12 ± 5	6	6
	1B	82 ± 17	84 ± 10	>125[d]	>125	>2	>1
	2B	64 ± 5	85 ± 18	>125	>125	>2	>1
	1C	47 ± 14	>83[d]	>83	>83	>2	
	2C	31 ± 1	78 ± 23	>62[d]	>62	>2	<1
	3C	2.9 ± 0.8	1.9 ± 0.4	>33[d]	>33	>11	>17
cisplatin		4.7 ± 1.8	1.1 ± 0.1	n.d.[e]	7.0 ± 0.8	1	6
doxorubicin		n.d.	1.0 ± 0.1	n.d.	n.d.		

[a]Effective concentrations of 50% in MDA-MB-231 (human breast adenocarcinoma), HCT116 (human colorectal carcinoma), CT26 (murine colon carcinoma), and MRC5 (human lung fibroblasts) determined by means of the MTT assay with the exposure time of 72 h. Values are means ± standard deviations obtained from at least three independent experiments. [b]The selectivity factor (SF) was determined as IC_{50}(MRC-5)/IC_{50}(MDA-MB-231). [c]The selectivity factor (SF) was determined as IC_{50}(MRC-5)/IC_{50}(HCT116) [d]The maximum tested concentrations were limited by the solubility of the compounds in DMSO. [e]Not determined.

Stability Studies. All Ru complexes were found to be poorly soluble in aqueous solutions and adequately soluble in DMSO; therefore, their subsequent biological analysis was performed in 1% DMSO in cell culture media. To ensure that investigated complexes are stable in DMSO and do not undergo decomposition or exchange of chlorido ligand, we investigated the stability of all complexes in DMSO-d_6 solvent using ^{1}H NMR spectroscopy for 72 h. The ^{1}H NMR signals did not undergo any changes within the tested period, indicating that complexes were stable in DMSO (Figures S25−S32). To assess the stability of compounds in aqueous media, we also performed UV−Vis spectrophotometric experiments in 1% DMSO diluted with either PBS or complete cell culture media (DMEM containing 10% FBS and 1% penicillin−streptomycin) diluted with H_2O in a ratio of 1:9 (Figures S33−S40). Complexes **1B**, **2A**, **3A**, and **2C** demonstrated high stability in PBS, reflected by only minor changes of intensity (Figures S34A−S36A and S39A). On the contrary, the UV−Vis spectra of **1A**, **2B**, and **1C** recorded after 72 h of incubation were characterized by the reduced intensities of the peaks at 285, 300, or 283 nm, respectively, and the appearance of isosbestic points at 405, 414, or 402 nm, respectively (Figures S33A, S37A, and S38A). The decrease of intensity might indicate the potential aggregation or precipitation of the complexes from the aqueous media. At the same time, the formation of isosbestic points is typically associated with the formation of new species. The UV−Vis spectrum of complex **3C** in PBS was characterized by the most significant changes, reflected by the marked increase of intensity of the peak centered at 275 nm and its slight shift to 287 nm after 72 h. Moreover, we observed the increase in intensity of a small peak at 395 nm and the formation of several isosbestic points (Figure S40A). Dissolution of compounds in complete cell culture media resulted in the quick formation of new species, as indicated by the appearance of several isosbestic points and other changes in the UV−Vis absorption bands after 24 h (Figures S33B−S40B). For example, in the case of complex **1A**, the strongest band centered at 285 nm demonstrated a time-dependent shift toward 280 nm and reduction of intensity, while small peaks at 396 and 376 nm were replaced by one broad peak centered at 375 nm (Figure S33B). Comparable changes were observed for all other tested complexes. Complex **3A** demonstrated the highest stability in PBS and complete cell culture media/H_2O mixture (Figures S35).

Anticancer Activity. The in vitro anticancer activity of the Ru complexes and their corresponding ligands was determined by the colorimetric MTT assay in the breast cancer cell line (MDA-MB-231) and colorectal cancer cell lines (HCT116 and CT26) with an exposure time of 72 h. The selectivity of the drug candidates toward the cancer cell lines was assessed in comparison with a non-cancerous human lung fibroblast cell line (MRC5). The maximum tested concentration was limited by the solubility of the compounds in DMSO. The IC_{50} values are listed in Table 1, and the concentration−effect curves are shown in Figure S41.

The activity of the ligands decreased in the following order: **A** ≈ **B** ≫ **C**. While **A** and **B** showed similar cytotoxicity in the low-micromolar concentration range, ligand **C** was non-cytotoxic, possibly due to its poor solubility in DMSO (≤0.2 mM). It should be noted that it was previously reported that dppz and its analogues were devoid of any anticancer activity against different cancer cell lines,[25,39,40] with the exception of ligand **A**, which was moderately cytotoxic against the HeLa cell line ($IC_{50(24\ h)}$ ≈ 60 μM).[39] The majority of the tested Ru complexes exhibited improved aqueous solubility but modest anticancer activity, similar to previously published Ru-dppz complexes.[17,19,21,25,26,41,42] Only **3A** and **3C** were cytotoxic in the low micromolar range in MDA-MB-231 and HCT116 cell lines in agreement with their higher aqueous stability. Interestingly, most of the tested compounds did not show any effects in the murine colon cancer CT26 cell line, indicating their selectivity toward human cancer cell lines. Overall, the cytotoxicity of the complexes showed the following trend in human cancer cell lines: **3** ≫ **2** ≈ **1**, suggesting the beneficial role of the cymene arene fragment. In agreement, previously published (cymene)Ru complexes with dppz ligands showed high cytotoxicity in the MDA-MB-231

https://doi.org/10.1021/acs.inorgchem.3c00570
Inorg. Chem. 2023, 62, 8188−8199

cell line, reflected by IC_{50} values between ca. 5 and 9 μM.[21,26] In general, the substitution of the arene had more profound effect on the cytotoxicity of the complexes than the variation of substituents in the dppz backbone. Additionally, we assessed the selectivity of all tested compounds toward cancer cell lines by comparing their IC_{50} values in MDA-MB-231 or HCT116 with IC_{50} values in the non-cancerous human lung fibroblast MRC5 cell line. As illustrated in Table 1, all drug candidates were more selective toward non-cancerous cells; in particular, **3C** was at least 17 times less toxic against MRC5 than HCT116. In comparison with clinically used anticancer drug cisplatin, **3A** and **3C** were more active against MDA-MB-231 breast cancer cells (*ca.* 10 and 7 times, respectively). Moreover, they were markedly more selective than cisplatin toward MRC5 (SF_{MDA} = 6, >11, and 0.3 for **3A**, **3C**, and cisplatin, respectively), as well as previously published structurally similar (arene)Ru-dppz complexes.[25,26] On the contrary, in HCT116 cells, cisplatin and another clinically used drug doxorubicin were more active than the majority of Ru complexes and comparably active to **3C** and ligands **A** and **B**. To understand whether the differences in the cytotoxicity between Ru complexes with different arene fragments were linked to their mechanism of action, we performed subsequent investigations of their DNA-degrading properties.

DNA Degradation. Previously, various metal complexes with dppz-based ligands, including half-sandwich complex $[(\eta^5\text{-}C_5Me_5)Ru(dppz)(NO)](OTf)$, were shown to affect the DNA mobility in gel electrophoresis experiments with plasmid DNA, indicating DNA cleavage.[43−45] Herein, we assessed the ability of Ru complexes **1A**−**3A** to affect cancer cell DNA using agarose gel-based DNA degradation assay in comparison with uncoordinated ligand **A** and clinically used DNA damaging agent doxorubicin. HCT116 colorectal cancer cells were incubated with the tested compounds at concentrations corresponding to their $IC_{50(72\ h)}$ values (and 3× IC_{50} value for doxorubicin) for 24 h. Subsequently, DNA was extracted, normalized, and assessed by 1% agarose gel electrophoresis. Quantification of the bands using BioRad Image Lab Software revealed the following trend in the efficacy of DNA degradation: **1A** ≈ **A** < **2A** < doxorubicin < **3A**. As can be seen in Figure 2, DNA extracted from the cells treated with **2A**, doxorubicin, and **3A** underwent considerable degradation as reflected by smearing band patterns. The remaining band intensities for **2A**, doxorubicin, and **3A** were ca. 79, 31, and 15% respectively, in comparison with untreated cells. The improved DNA degradation of **3A** in comparison with equally cytotoxic ligand **A** might be related to the interactions of the DNA nucleobases with an Ru center.[46] On the other hand, DNA extracted from cells treated with **1A** and **A** remained relatively intact, although ligand **A** caused some degree of DNA smearing, indicating initial fragmentation of high-molecular weight DNA. Since all compounds were used at equipotent concentrations, the most prominent DNA degradation caused by (cymene)Ru-dppz complex **3A** might be one of the underlying causes of its highest cytotoxicity among the tested complexes.

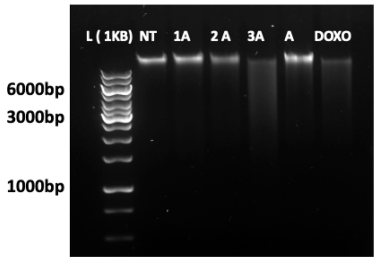

Figure 2. Detection of DNA degradation using 1% agarose gel electrophoresis. HCT116 cells were treated with complexes **1A**−**3A** and **A** at their respective 1 × IC_{50} values and doxorubicin as a positive control at a 3 × IC_{50} value for 24 h. DNA was normalized using a NanoDrop One/OneC Microvolume UV−Vis spectrophotometer, and 200 ng per sample was loaded into each well (lane 1, 1 kb DNA ladder; lane 2, untreated cells (NT); lane 3, **1A**; lane 4, **2A**; lane 5, **3A**; lane 6, **A**; lane 7, doxorubicin (DOXO)). Gel imaging was performed under UV light using a ChemiDoc Touch Imaging System (BioRad).

ROS Detection. It is known that superoxide anionic radicals, hydroxyl free radicals, and other ROS are produced as a result of one or more oxygen electrons being reduced by cellular enzymes or in the mitochondrial respiratory system.[47] These molecules play an important function in cellular signaling for various biological processes; however, an excess of free radicals might lead to DNA damage and cell death as well as DNA mutations and carcinogenesis.[48] In cancer cells, ROS production is elevated due to their higher metabolic rate compared to normal cells.[49] Various structurally different Ru complexes were shown to induce ROS-mediated cancer cell death.[50,51] However, typically ROS experiments were carried out after prolonged drug exposure (12−48 h);[21,50] thus, the ROS observed in drug-treated cancer cells might be the consequence of cell damage caused by other mechanisms. Based on the results of cyclic voltammetry experiments, **1A**−**3A**, **1B**, **2B**, and **1C**−**3C** were electrochemically active, and the biologically accessible reduction was dppz ligand-based. Therefore, we expected that these complexes could initiate ROS insult after a short timepoint, leading to DNA damage and cancer cell death. We used the triple-staining protocol with nuclear staining Hoechst dye, mitochondria-specific Mitotracker Red CMXRos dye, and ROS-sensitive DCFDA dye. HCT116 cells were treated with complex **3A** and respective ligand **A** for 4 h, and live cell images were obtained using confocal microscopy. As expected, **3A** caused an increase in mitochondrial ROS production reflected by enhanced green DCF fluorescence colocalized with mitochondrial staining. On the other hand, **A** did not induce marked ROS insult (Figure 3). These results suggest that mitochondrial ROS production might be one of the underlying causes of **3A**-induced cancer cell death. Additionally, to quantify the amount of ROS generated by the compounds of interest, we performed flow cytometric analysis of drug-treated HCT116 cells (Figure S42). In agreement with the microscopic studies, ligand **A** was characterized by an insignificant increase of DCF fluorescence, while **3A** caused more than 8-fold increase in DCF fluorescence similar to H_2O_2 (100 μM, cell-free, positive control). Inspired by promising in vitro activity of **3A**, we subsequently performed an in vivo efficacy study using Balb/C mice.

In Vivo Experiments. Initially, we performed a pilot acute toxicity study on BALB/c mice to determine the appropriate dose of tested compounds for the subsequent efficacy study. Animals (n = 12) were randomly distributed into four groups and were intraperitoneally injected with drug candidates or respective vehicle (three injections within 1 week; Group 1: 10 mg/kg of **3A**, Group 2: 20 mg/kg of **3A**, Group 3: 0.8 mg/kg of **A**, and Group 4: vehicle). The injected dose of the ligand

https://doi.org/10.1021/acs.inorgchem.3c00570
Inorg. Chem. 2023, 62, 8188−8199

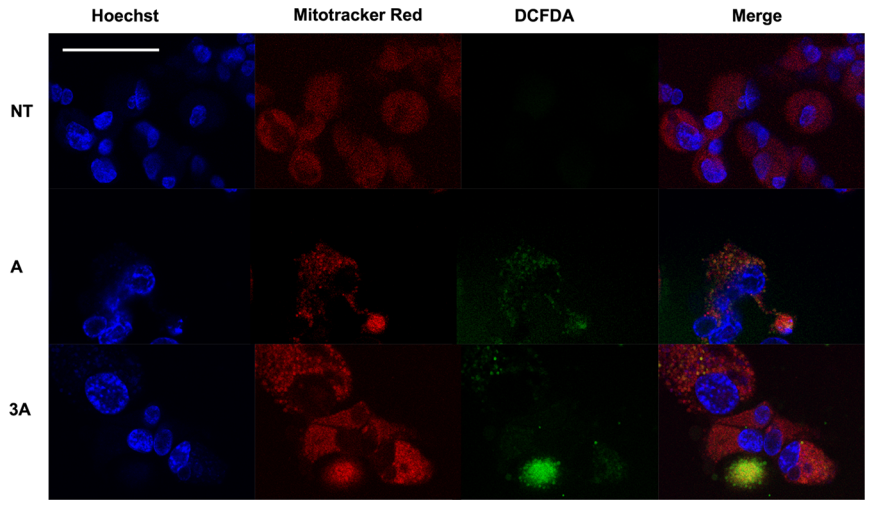

Figure 3. ROS detection using live cell confocal microscopy imaging. HCT116 cells were stained with H_2DCFDA (excitation/emission wavelengths of 504 nm/525 nm) for 15 min, incubated with complex **3A** (1 × IC_{50}) and **A** (1 × IC_{50}) for 4 h. Hoechst 33342 dye (excitation/emission wavelength of 350/461) and Mitotracker Red CMXRos dye (excitation/emission wavelengths of 579 nm/599 nm) were used for nuclear and mitochondrial staining, respectively. Images were acquired using a Leica confocal laser scanning microscope and analyzed via Microscope Software Platform LAS X Life Science. The scale bar represents 50 μm. NT, untreated cells.

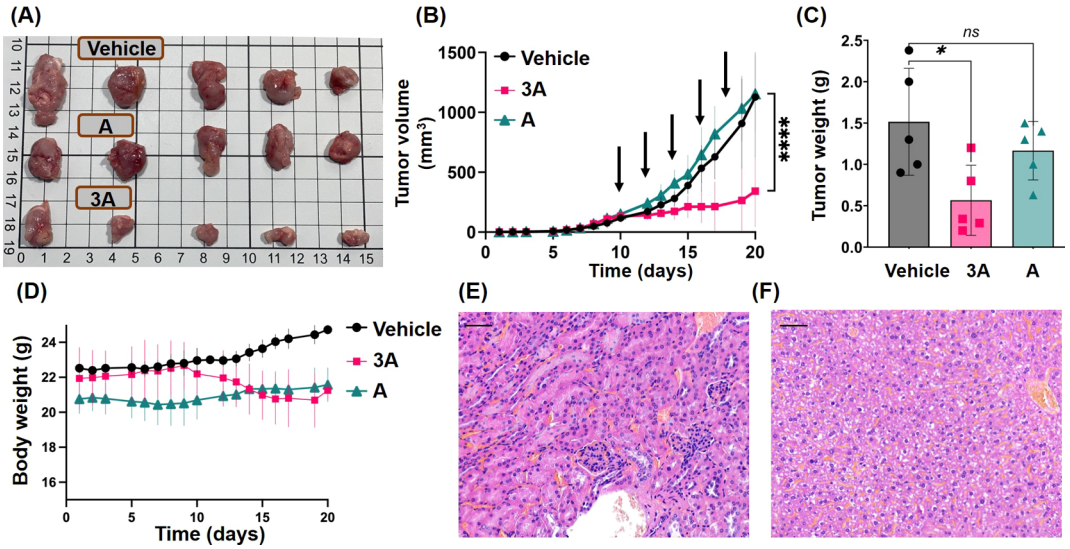

Figure 4. Effects of **A** and **3A** on CT26 tumor growth in vivo. (A) Representative tumor images at the endpoint (day 20) after five i.p. injections of **A**, **3A**, or vehicle. (B) Time-dependent tumor growth in CT26 tumor-bearing Balb/C mice. Starting from day 8, the tumors became palpable and their volume was measured by a caliper weekly. Mice (n = 5) were treated with **A** at 0.8 mg kg^{-1}, **3A** at 8 mg kg^{-1}, or respective vehicle (DMSO/Cremophor EL in sterile saline) via the i.p. route every other day (arrows represent the injection days). (C) Weights of the isolated tumors shown in Figure 4A. (D) Body weight changes of Balb/C mice during the treatment. (E) Representative H&E-stained kidney tissue of a **3A**-treated mouse, demonstrating normal kidney structure. (F) Representative H&E-stained liver tissue of a **3A**-treated mouse, demonstrating preserved liver tissue architecture. The scale bar represents 50 μm. Statistical analysis was performed by (B) two-way ANOVA test with Dunnett's post hoc analysis or (C) unpaired t test using GraphPad Prism 9 software (GraphPad Software Inc., CA) with $p < 0.05$ considered as significant (*$p < 0.05$, ****$p < 0.0001$, ns: not significant).

was severely limited by its precipitation from aqueous solutions. However, the addition of Cremophor EL (final concentration not exceeding 1−3%) ensured sufficient solubility of drug candidates in physiological saline. Importantly, the solubility of Ru complex **3A** allowed for testing at significantly higher doses (up to 20 mg/kg), which indicates one of the advantages of Ru coordination. The weight changes and clinical signs of toxicity were monitored daily. Mice in the ligand and control groups did not reveal any signs of toxicity during the whole observation period. In Group 2, two mice were found dead after the first injection, while in Group 1, we observed ∼10% weight loss in one mouse after the second injection. Therefore, we chose 8 mg/kg of **3A** for subsequent in vivo efficacy studies. Next, we established a mouse colorectal cancer CT26 xenograft model. Animals (n = 15) were randomly divided into three groups as follows: Group 1, **3A** (8 mg/kg); Group 2, **A** (0.8 mg/kg); Group 3, vehicle (1% DMSO/Cremophor EL in sterile physiological saline). As soon as the tumors became palpable (day 10), the mice were intraperitoneally injected with drug candidates or the vehicle every second day for 10 consecutive days (overall five injections). When the tumor volume in the control group

https://doi.org/10.1021/acs.inorgchem.3c00570
Inorg. Chem. 2023, 62, 8188−8199

reached 1500 mm^3, the animals were humanely sacrificed and the tumors, kidneys, and livers were harvested for further histological examination. We observed disease stabilization in the group of **3A**-treated mice since there was a significant tumor growth inhibition after the beginning of treatment (Figures 4A−C). The histological examination of tumor tissues from **3A**-treated mice revealed solid sheets of high-grade carcinoma with low levels of necrosis (Figure S43). Meanwhile, the vehicle-treated and ligand-treated groups were characterized by disease progression, reflected by the *ca.* 7−8-fold increase of tumor size after the beginning of the treatment, as well as high levels of necrosis, characteristic for late stages of advanced solid tumors and highly proliferative tumors (Figures S44 and S45). At the endpoint, the **3A**-treated tumors were *ca.* 3 and 4 times smaller than in the vehicle- and ligand-treated groups, respectively (Figures 4A−C). Importantly, no statistically significant differences were observed between the vehicle- and ligand-treated groups, suggesting that the presence of the (arene)Ru fragment is crucial for its therapeutic efficacy. During the whole length of the experiment, all mice were bright, alert, and responsive and did not exhibit any clinical signs of toxicity (body weight changes not more than 7%; Figure 4D). In agreement, the kidneys harvested from all three groups demonstrated normal structures without significant microscopic structural changes (Figure 4E and Figure S46). In livers from all three groups, several areas of hemorrhages were detected as well as nuclei polymorphism, sinusoidal dilatation, and cytoplasm vacuolization; however, the liver tissue architecture was preserved in all groups (Figure 4F and Figure S46), indicating that the observed effects were not caused by the drug treatment.

CONCLUSIONS

In this work, we prepared eight Ru(II)-arene complexes with three different arene fragments and three dppz-based ligands. The cytotoxicity of the complexes against the MDA-MB-231 and HCT116 breast cancer cell lines varied from low micromolar to high micromolar concentrations. We demonstrated that the cytotoxicity of the complexes was more strongly dependent on the Ru(II)-arene fragment than substituents in the dppz backbone. The cytotoxicity of the complexes decreased in the following order: **3** ≫ **2** ≈ **1**, suggesting the beneficial role of the *p*-cymene fragment. To the best of our knowledge, (*p*-cymene)Ru(II) complexes **3A** and **3C** represent one of the most cytotoxic half-sandwich Ru-dppz complexes reported in the literature (IC_{50} values ≈ 2−3 μM). The variation of the arene fragment drastically affected the stability of the complexes and their ability to degrade DNA in colorectal cancer cells. Only **3A**, but not **1A** and **2A**, degraded DNA to a similar extent as a clinically used anticancer agent doxorubicin. Further mechanistic investigations revealed that uncoordinated dppz ligand **A** and its respective Ru(II) complex **3A** induced deadly ROS production in the mitochondria only after 4 h, which was in agreement with their electrochemical activity. The ROS production induced by **3A** was considerably stronger in the case if the dppz ligand. Additionally, all tested Ru complexes demonstrated some degree of selectivity toward healthy MRC5 lung fibroblasts; however, the origin of this selectivity is yet to be determined. The in vivo efficacy of a dppz ligand was hindered by its poor solubility in aqueous buffers even in the presence of Cremophor EL, while the coordination of the Ru(II)-arene fragment allowed for a 10-fold increase of the tested dose (0.8 mg/kg for **A** vs 8 mg/kg for **3A**). The vehicle-treated and ligand **A**-treated mice were characterized by rapid tumor growth and the occurrence of necrosis, characteristic of rapidly proliferating tumors, as confirmed by the histopathological analysis. On the contrary, **3A** significantly reduced the tumor size and tumor weight in CT26-bearing mice without inducing any toxic side effects. While the cytotoxicity of **3A** might not be sufficient for the successful preclinical development of this drug candidate, the results of this work justify the subsequent studies on other series of anticancer half-sandwich Ru(II)-dppz complexes and further elucidation of their structure−activity relationships.

ASSOCIATED CONTENT

Supporting Information

The Supporting Information is available free of charge at https://pubs.acs.org/doi/10.1021/acs.inorgchem.3c00570.

Electrochemical data for dppz ligands **A**−**C** and their respective Ru(II) complexes **1A**−**3A**, **1B**, **2B**, and **1C**−**3C**; high-resolution ESI-MS spectra of **1A**−**3A**, **1B**, **2B**, and **1C**−**3C**; ^{1}H and ^{13}C NMR spectra of **1A**−**3A**, **1B**, **2B**, and **1C**−**3C**; ^{1}H NMR study on the stability of **1A**−**3A**, **1B**, **2B**, and **1C**−**3C** in DMSO-d_6 for 24 h; UV−Vis study on the stability of **1A**−**3A**, **1B**, **2B**, and **1C**−**3C** in 1% DMSO in PBS or complete cell culture media/H_2O in a ratio of 1:9 for 24 h; concentration−effect curves for **1A**−**3A**, **1B**, **2B**, and **1C**−**3C** in MDA-MB-231 and HCT116 cell lines upon 72 h of exposure; flow cytometry analysis of drug-induced intracellular ROS generation; H&E-stained tumor sections in vehicle-, ligand **A**- and Ru complex **3A**-treated groups; H&E-stained kidney and liver sections in vehicle- and ligand **A**-treated groups (PDF)

AUTHOR INFORMATION

Corresponding Authors

Sanja Grgurić-Šipka − *Faculty of Chemistry, University of Belgrade, 11000 Belgrade, Serbia*; Email: sanjag@chem.bg.ac.rs

Maria V. Babak − *Drug Discovery Lab, Department of Chemistry, City University of Hong Kong, Hong Kong SAR 999077, People's Republic of China*; orcid.org/0000-0002-2009-7837; Email: mbabak@cityu.edu.hk

Authors

Stefan Nikolić − *Innovative Centre of the Faculty of Chemistry Belgrade, University of Belgrade, 11000 Belgrade, Serbia*

Jemma Arakelyan − *Drug Discovery Lab, Department of Chemistry, City University of Hong Kong, Hong Kong SAR 999077, People's Republic of China*

Vladimir Kushnarev − *Drug Discovery Lab, Department of Chemistry, City University of Hong Kong, Hong Kong SAR 999077, People's Republic of China*

Samah Mutasim Alfadul − *Drug Discovery Lab, Department of Chemistry, City University of Hong Kong, Hong Kong SAR 999077, People's Republic of China*

Dalibor Stanković − *Faculty of Chemistry, University of Belgrade, 11000 Belgrade, Serbia*

Yaroslav I. Kraynik − *Drug Discovery Lab, Department of Chemistry, City University of Hong Kong, Hong Kong SAR 999077, People's Republic of China*

Complete contact information is available at:

https://doi.org/10.1021/acs.inorgchem.3c00570
Inorg. Chem. 2023, 62, 8188−8199

https://pubs.acs.org/10.1021/acs.inorgchem.3c00570

Notes

The authors declare no competing financial interest.

■ ACKNOWLEDGMENTS

This work was supported by the City University of Hong Kong (projects 9610518 and 7005614) and the Ministry of Education, Science and Technological Development of the Republic of Serbia (contract numbers: 451-03-68/2023-14/200288 and 451-03-47/2023-01/200168). M.V.B. acknowledges Ho-Jung Choe for generating the TOC artwork.

■ REFERENCES

(1) Alessio, E.; Messori, L. NAMI-A and KP1019/1339, Two Iconic Ruthenium Anticancer Drug Candidates Face-to-Face: A Case Story in Medicinal Inorganic Chemistry. *Molecules* **2019**, *24*, 1995.

(2) Tremlett, W. D. J.; Goodman, D. M.; Steel, T. R.; Kumar, S.; Wieczorek-Błauż, A.; Walsh, F. P.; Sullivan, M. P.; Hanif, M.; Hartinger, C. G. Design concepts of half-sandwich organoruthenium anticancer agents based on bidentate bioactive ligands. *Coord. Chem. Rev.* **2021**, *445*, No. 213950.

(3) Li, J.; Guo, L.; Tian, Z.; Zhang, S.; Xu, Z.; Han, Y.; Li, R.; Li, Y.; Liu, Z. Half-Sandwich Iridium and Ruthenium Complexes: Effective Tracking in Cells and Anticancer Studies. *Inorg. Chem.* **2018**, *57*, 13552−13563.

(4) Chen, F.; Romero-Canelón, I.; Habtemariam, A.; Song, J.-I.; Banerjee, S.; Clarkson, G. J.; Song, L.; Prokes, I.; Sadler, P. J. Effect of cysteine thiols on the catalytic and anticancer activity of Ru(ii) sulfonyl-ethylenediamine complexes. *Dalton Trans.* **2022**, *51*, 4447−4457.

(5) Soldevila-Barreda, J. J.; Romero-Canelón, I.; Habtemariam, A.; Sadler, P. J. Transfer hydrogenation catalysis in cells as a new approach to anticancer drug design. *Nat. Commun.* **2015**, *6*, 6582.

(6) Fan, Z.; Xie, J.; Kushwaha, R.; Liang, S.; Li, W.; Mandal, A. A.; Wei, L.; Banerjee, S.; Huang, H. Anticancer Screening of Ru(II) Photoredox Catalysts at Single Cancer Cell Level. *Chem. − Asian J.* , e202300047.

(7) Chow, M. J.; Licona, C.; Pastorin, G.; Mellitzer, G.; Ang, W. H.; Gaiddon, C. Structural tuning of organoruthenium compounds allows oxidative switch to control ER stress pathways and bypass multidrug resistance. *Chem. Sci.* **2016**, *7*, 4117−4124.

(8) Chow, M. J.; Babak, M. V.; Wong, D. Y.; Pastorin, G.; Gaiddon, C.; Ang, W. H. Structural Determinants of p53-Independence in Anticancer Ruthenium-Arene Schiff-Base Complexes. *Mol. Pharmaceutics* **2016**, *13*, 2543−2554.

(9) Chao, H.; Li, G. Y.; Sun, L.; Ji, L.-N. Ruthenium(II) Complexes with Dppz: From Molecular Photoswitch to Biological Applications. *Dalton Trans.* **2016**, *45*, 13261−13276.

(10) Bonnett, R. Photosensitizers of the porphyrin and phthalocyanine series for photodynamic therapy. *Chem. Soc. Rev.* **1995**, *24*, 19−33.

(11) Friedman, A. E.; Chambron, J. C.; Sauvage, J. P.; Turro, N. J.; Barton, J. K. A molecular light switch for DNA: Ru(bpy)2(dppz)2+. *J. Am. Chem. Soc.* **1990**, *112*, 4960−4962.

(12) Schatzschneider, U.; Niesel, J.; Ott, I.; Gust, R.; Alborzinia, H.; Wölfl, S. Cellular Uptake, Cytotoxicity, and Metabolic Profiling of Human Cancer Cells Treated with Ruthenium(II) Polypyridyl Complexes [Ru(bpy)2(NN)]Cl2 with NN=bpy, phen, dpq, dppz, and dppn. *ChemMedChem* **2008**, *3*, 1104−1109.

(13) Pierroz, V.; Joshi, T.; Leonidova, A.; Mari, C.; Schur, J.; Ott, I.; Spiccia, L.; Ferrari, S.; Gasser, G. Molecular and cellular characterization of the biological effects of ruthenium(II) complexes incorporating 2-pyridyl-2-pyrimidine-4-carboxylic acid. *J. Am. Chem. Soc.* **2012**, *134*, 20376−20387.

(14) Tan, L. F.; Wang, F.; Su, G. J.; Chao, H.; Zhang, S. Synthesis and spectroscopic DNA binding studies of [Ru(phen)2(tbtc)]2+ and [Ru(2,9-dmp)2(tbtc)]2+.*Acta A Mol. Biomol. Spectrosc.* **2008**, *71*, 1181−1187.

(15) Di Pietro, M. L.; La Ganga, G.; Nastasi, F.; Puntoriero, F. Ru(II)-Dppz Derivatives and Their Interactions with DNA: Thirty Years and Counting. *Appl. Sci.* **2021**, *11*, 3038.

(16) Huang, H.; Zhang, P.; Yu, B.; Chen, Y.; Wang, J.; Ji, L.; Chao, H. Targeting nucleus DNA with a cyclometalated dipyridophenazineruthenium(II) complex. *J. Med. Chem.* **2014**, *57*, 8971−8983.

(17) Wachter, E.; Moyá, D.; Parkin, S.; Glazer, E. C. Ruthenium Complex "Light Switches" that are Selective for Different G-Quadruplex Structures. *Chem. − Eur. J.* **2016**, *22*, 550−559.

(18) Ni, W.; Liu, X.; Tan, L. Binding properties of chiral ruthenium(II) complexes Λ- and Δ-[Ru(bpy)(2)dppz-11-CO(2)-Me](2+) toward the triplex RNA poly(U)•poly(A)*poly(U). *J. Inorg. Biochem.* **2018**, *186*, 51−59.

(19) Chen, L.; Li, G.; Peng, F.; Jie, X.; Dongye, G.; Cai, K.; Feng, R.; Li, B.; Zeng, Q.; Lun, K.; Chen, J.; Xu, B. The induction of autophagy against mitochondria-mediated apoptosis in lung cancer cells by a ruthenium (II) imidazole complex. *Oncotarget* **2016**, *7*, 80716−80734.

(20) Hu, L.; Bian, Z.; Li, H.; Han, S.; Yuan, Y.; Gao, L.; Xu, G. [Ru(bpy)(2)dppz](2+) Electrochemiluminescence Switch and Its Applications for DNA Interaction Study and Label-free ATP Aptasensor. *Anal. Chem.* **2009**, *81*, 9807−9811.

(21) Kar, B.; Paira, P. One pot three component synthesis of DNA targeting phototoxic Ru(II)- p -cymene dipyrido[3,2-a:2′,3′- c]phenazine analogues. *Dalton Trans.* **2022**, *51*, 15686-15695.22.

(22) Roy, N.; Sen, U.; Ray Chaudhuri, S.; Muthukumar, V.; Moharana, P.; Paira, P.; Bose, B.; Gauthaman, A.; Moorthy, A. Mitochondria specific highly cytoselective iridium(iii)−Cp* dipyridophenazine (dppz) complexes as cancer cell imaging agents. *Dalton Trans.* **2021**, *50*, 2268−2283.

(23) Ganeshpandian, M.; Palaniandavar, M.; Murugananthan, A.; Ghosh, S. K.; Riyasdeen, A.; Akbarsha, M. A. Ruthenium(II)−arene complexes of diimines: Effect of diimine intercalation and hydrophobicity on DNA and protein binding and cytotoxicity. *App. Organomet. Chem.* **2018**, *32*, No. e4154.

(24) Frodl, A.; Herebian, D.; Sheldrick, W. S. Coligand tuning of the DNA binding properties of bioorganometallic (η6-arene)ruthenium-(ii) complexes of the type [(η6-arene)Ru(amino acid)(dppz)]n+ (dppz = dipyrido[3,2-a:2′,3′-c]phenazine), n = 1−3. *J. Chem. Soc., Dalton Trans.* **2002**, *19*, 3664−3673.

(25) Nikolić, S.; Rangasamy, L.; Gligorijević, N.; Aranđelović, S.; Radulović, S.; Gasser, G.; Grgurić-Sipka, S. Synthesis, characterization and biological evaluation of novel Ru(II)−arene complexes containing intercalating ligands. *J. Inorg. Biochem.* **2016**, *160*, 156−165.

(26) Savić, A.; Gligorijević, N.; Aranđelović, S.; Dojčinović, B.; Kaczmarek, A. M.; Radulović, S.; Van Deun, R.; Van Hecke, K. Antitumor activity of organoruthenium complexes with chelate aromatic ligands, derived from 1,10-phenantroline: Synthesis and biological activity. *J. Inorg. Biochem.* **2020**, *202*, No. 110869.

(27) Betanzos-Lara, S.; Novakova, O.; Deeth, R. J.; Pizarro, A. M.; Clarkson, G. J.; Liskova, B.; Brabec, V.; Sadler, P. J.; Habtemariam, A. Bipyrimidine ruthenium(II) arene complexes: structure, reactivity and cytotoxicity. *J. Biol. Inorg. Chem.* **2012**, *17*, 1033−1051.

(28) Matveevskaya, V. V.; Pavlov, D. I.; Sukhikh, T. S.; Gushchin, A. L.; Ivanov, A. Y.; Tennikova, T. B.; Sharoyko, V. V.; Baykov, S. V.; Benassi, E.; Potapov, A. S. Arene−Ruthenium(II) Complexes Containing 11H-Indeno[1,2-b]quinoxalin-11-one Derivatives and Tryptanthrin-6-oxime: Synthesis Characterization, Cytotoxicity, and Catalytic Transfer Hydrogenation of Aryl Ketones. *ACS Omega* **2020**, *5*, 11167−11179.

(29) Zhao, X.; Li, L.; Yu, G.; Zhang, S.; Li, Y.; Wu, Q.; Huang, X.; Mei, W. Nucleus-enriched Ruthenium Polypyridine Complex Acts as a Potent Inhibitor to Suppress Triple-negative Breast Cancer Metastasis In vivo. *Comput. Struct. Biotechnol. J.* **2019**, *17*, 21−30.

(30) Jensen, S. B.; Rodger, S. J.; Spicer, M. D. Facile preparation of η6-p-cymene ruthenium diphosphine complexes. Crystal structure of

[(η6-p-cymene)Ru(dppf)Cl]PF6. *J. Organomet. Chem.* **1998**, *556*, 151−158.
(31) Molphy, Z.; Prisecaru, A.; Slator, C.; Barron, N.; McCann, M.; Colleran, J.; Chandran, D.; Gathergood, N.; Kellett, A. Copper Phenanthrene Oxidative Chemical Nucleases. *Inorg. Chem.* **2014**, *53*, 5392−5404.
(32) Balu, K.; Velmurugan, R.; Jothivel, S.; Swaminathan, M. An efficient protocol for the green synthesis of quinoxaline and dipyridophenazine derivatives at room temperature using sulfated titania. *Catal. Commun.* **2010**, *11*, 997−1002.
(33) Shigehiro, T.; Yagi, S.; Maeda, T.; Nakazumi, H.; Fujiwara, H.; Sakurai, Y. Novel 10,13-disubstituted dipyrido[3,2-a:2′,3′-c]-phenazines and their platinum(II) complexes: Highly luminescent ICT-type fluorophores based on D-A-D structures. *Tetrahedron Lett.* **2014**, *55*, 5195−5198.
(34) Tan, L.-F.; Wang, F.; Chao, H.; Zhang, S.; Fei, J.-J.; Ji, L.-N. DNA Interactions of the Functionalized (Mixed Polypyridine)-ruthenium(II) Complex Bis(2,2′-bipyridine-]κ]$N_{1'}$,]κ]$N_{1'}$)(methyl dipyrido[3,2-*a* : 2′,3′-c]phenazine-11-carboxylate-]κ]N_4,]κ]N_5)-ruthenium$^{(2+)}$ ([Ru(bpy)$_2$(dppz-11-CO$_2$Me)]$^{2+}$). *Helv. Chim. Acta* **2008**, *91*, 1251−1260.
(35) Fischer, A. H.; Jacobson, K. A.; Rose, J.; Zeller, R. Hematoxylin and eosin staining of tissue and cell sections. *CSH Protoc.* **2008**, pdb.prot4986.
(36) Greaves, P., Digestive System, in: P., Greaves (Ed.) *Histopathology of Preclinical Toxicity Studies (Fourth Edition)*; Academic Press, Boston, 2012, 325−431
(37) Kleineweischede, A.; Mattay, J. Synthesis, spectroscopic and electrochemical studies of a series of transition metal complexes with amino- or bis(bromomethyl)-substituted dppz-ligands: Building blocks for fullerene-based donor−bridge−acceptor dyads. *J. Organomet. Chem.* **2006**, *691*, 1834−1844.
(38) Jungwirth, U.; Kowol, C. R.; Keppler, B. K.; Hartinger, C. G.; Berger, W.; Heffeter, P. Anticancer activity of metal complexes: involvement of redox processes. *Antioxid. Redox Signaling* **2011**, *15*, 1085−1127.
(39) Musib, D.; Banerjee, S.; Garai, A.; Soraisam, U.; Roy, M. Synthesis, Theory and In Vitro Photodynamic Activities of New Copper(II)-Histidinito Complexes. *ChemistrySelect* **2018**, *3*, 2767−2775.
(40) Villarreal, W.; Colina-Vegas, L.; Visbal, G.; Corona, O.; Corrêa, R. S.; Ellena, J.; Cominetti, M. R.; Batista, A. A.; Navarro, M. Copper(I)−Phosphine Polypyridyl Complexes: Synthesis, Characterization, DNA/HSA Binding Study, and Antiproliferative Activity. *Inorg. Chem.* **2017**, *56*, 3781−3793.
(41) Zhou, Q.; Lei, W.; Chen, Y.; Li, C.; Hou, Y.; Zhang, B.; Wang, X. Ruthenium(II)-arene complexes with strong fluorescence: insight into the underlying mechanism. *Chemistry* **2012**, *18*, 8617−8621.
(42) Schäfer, S.; Ott, I.; Gust, R.; Sheldrick, W. S. Influence of the Polypyridyl (pp) Ligand Size on the DNA Binding Properties, Cytotoxicity and Cellular Uptake of Organoruthenium(II) Complexes of the Type [(η6-C6Me6)Ru(L)(pp)]n+ [L = Cl, n = 1; L = (NH2)2CS, n = 2]. *Eur. J. Inorg. Chem.* **2007**, *2007*, 3034−3046.
(43) Schoch, T. K.; Hubbard, J. L.; Zoch, C. R.; Yi, G.-B.; Sørlie, M. Synthesis and Structure of the Ruthenium(II) Complexes [(η-C5Me5)Ru(NO)(bipy)]2+ and [(η-C5Me5)Ru(NO)(dppz)]2+. DNA Cleavage by an Organometallic dppz Complex (bipy = 2,2‘-Bipyridine; dppz = Dipyrido[3,2-a:2′,3′-c]phenazine). *Inorg. Chem.* **1996**, *35*, 4383−4390.
(44) Herebian, D.; Sheldrick, W. S. Synthesis and DNA binding properties of bioorganometallic (η5-pentamethylcyclopentadienyl)-iridium(iii) complexes of the type [(η5-C5Me5)Ir(Aa)(dppz)]+ (dppz = dipyrido[3,2-a:2′,3′-c]phenazine, n = 1−3), with S-coordinated amino acids (Aa) or peptides. *J. Chem. Soc., Dalton Trans.* **2002**, *6*, 966−974.
(45) Cunningham, M.; McCrate, A.; Nielsen, M.; Swavey, S. Highly Efficient Visible-Light-Induced Photocleavage of DNA by a Ruthenium-Substituted Fluorinated Porphyrin. *Eur. J. Inorg. Chem.* **2009**, *11*, 1521−1525.
(46) Lozano, H. J.; Busto, N.; Espino, G.; Carbayo, A.; Leal, J. M.; Platts, J. A.; García, B. Interstrand DNA covalent binding of two dinuclear Ru(ii) complexes. Influence of the extra ring of the bridging ligand on the DNA interaction and cytotoxic activity. *Dalton Trans.* **2017**, *46*, 3611−3622.
(47) Jakubczyk, K.; Dec, K.; Kałduńska, J.; Kawczuga, D.; Kochman, J.; Janda, K. Reactive oxygen species - sources, functions, oxidative damage. *Pol. Merkur.* **2020**, *48*, 124−127.
(48) Sinenko, S. A.; Starkova, T. Y.; Kuzmin, A. A.; Tomilin, A. N. Physiological Signaling Functions of Reactive Oxygen Species in Stem Cells: From Flies to Man. *Front. Cell Dev. Biol.* **2021**, *9*, No. 714370.
(49) Aggarwal, V.; Tuli, H. S.; Varol, A.; Thakral, F.; Yerer, M. B.; Sak, K.; Varol, M.; Jain, A.; Khan, M. A.; Sethi, G. Role of Reactive Oxygen Species in Cancer Progression: Molecular Mechanisms and Recent Advancements. *Biomolecules* **2019**, *9*, 735.
(50) Chen, J. C.; Zhang, Y.; Jie, X. M.; She, J.; Dongye, G. Z.; Zhong, Y.; Deng, Y. Y.; Wang, J.; Guo, B. Y.; Chen, L. M. Ruthenium(II) salicylate complexes inducing ROS-mediated apoptosis by targeting thioredoxin reductase. *J. Inorg. Biochem.* **2019**, *193*, 112−123.
(51) Gruia, M. I.; Negoita, V.; Vasilescu, M.; Panait, M.; Gruia, I. O. N.; Velescu, B. S.; Uivarosi, V. Biochemical Action of New Complexes of Ruthenium with Quinolones as Potential Antitumor Agents. *Anticancer Res.* **2015**, *35*, 3371.

https://doi.org/10.1021/acs.inorgchem.3c00570
Inorg. Chem. 2023, 62, 8188−8199